Combining model-free and model-based Angle of Attack estimation for small fixed-wing UAVs using a standard sensor suite

Andreas Wenz *, Tor Arne Johansen*, Andrea Cristofaro*
*Centre for Autonomous Marine Operations and Systems
Department of Engineering Cybernetics
Norwegian University of Science and Technology, Trondheim, Norway

***Abstract*— We propose to estimate steady and turbulent wind velocities and aerodynamic coefficients of a fixed-wing Unmanned Aerial Vehicle (UAV) by using frequency separation as well as kinematic, aerodynamic and wind models combined in an Extended Kalman Filter (EKF). With these estimates it is possible to calculate the angle of attack and the magnitude of the airspeed. Avoiding the need for prior knowledge of UAV parameters, the proposed method utilizes only sensor information that is part of a standard sensor suite, which consists of a GNSS, an IMU and a pitot-static tube, and attitude information obtained from these sensors. An observability analysis shows that attitude changes are necessary during the initialization phase and from time to time during the flight. Simulation results indicate that, with typical sensor accuracy, the estimates are close to the reference values of the aerodynamic coefficients and wind velocities and is capable of estimating the Angle of Attack with an RMSE of 0.33°, the Sideslip Angle with an Root Mean Square Error (RMSE) of 3.21 °and the airspeed with an RMSE of 0.23 m/s.**

I. Introduction

For a fixed-wing aircraft the angle of attack (α), the side slip angle (β) and the airspeed (V_a) are useful variables to characterize flight performance and safety in both normal and abnormal conditions, such as stall and strong and turbulent winds. Large aircraft are usually equipped with vanes or multi hole pitot-static tubes which are able to deliver an accurate and redundant estimate of these variables. However on small unmanned aerial vehicles (UAVs) the constraints on size, weight and costs are considerably stronger and sensors solely designated to measure α, β and V_a are typically not practical with using current technology. One might therefore apply aerodynamic models assuming the knowledge of aerodynamic coefficients, such as the lift and drag coefficients (see e.g. [2]). In practice this can be quite difficult, since these coefficients might change from one mission to another, due to different payloads or due to individual differences in UAV configurations within a fleet of supposedly equal UAVs. Changes might even occur during one mission due to structural changes such as icing. In this paper the estimation of airflow variables α, β and V_a and the simultaneous estimation of the aerodynamic coefficients will be studied. For this only a standard sensor suite, containing a GNSS (Global Navigation Satellite System), an IMU (Inertial Measurement Unit) and a pitot-static tube will be utilized. The method fuses these data sources with kinematic, aerodynamic and stochastic wind models in an EKF.

Several methods have been recently proposed to estimate the airflow variables and aerodynamic coefficients. One popular methods is the EKF, which has been used in [3] , [9], [11], and the Unscented Kalman Filter which has been applied to the problem in [12], [4]. Tian et.al [15] compare the use of an EKF, Output Error Minimization and a Complimentary Filter to improve measurements of the airflow variables obtained from a multi-directional pitot tube. In [10] kinematic vehicle models are used together with IMU, GNSS and multi-directional airspeed sensors to estimate the wind field. [13] propose a method using optical flow measurements. A hybrid system approach using Bayesian estimation is presented in [14], and achieving promising results. However in the described method a detailed model of the aerodynamics is used and the parameters for this might not always be available.

This paper builds up on [6], where the information from the above mentioned sensor suite was used together with kinematic relationships to estimate wind velocities and from these calculate the aerodynamic variables in a Kalman Filter. The underlying wind model assumed steady slowly changing wind. It is worth mentioning that the method does not rely on knowledge of any parameters of the UAV, what makes it easy to implement without the need to adapt to any platform and payload changes.

The main contribution of this paper is the extension of the above described method by combining the measurements of the pitot tube with those of an accelerometer to separately estimate steady and turbulent wind velocities in inertial frame using frequency separation and a Dryden model [1]. We will show how this can be achieved without needing prior knowledge of the aircraft and only using kinematic and simplified aerodynamic relationships within an Extended Kalman Filter. In contrast to previous work, the needed aerodynamic parameters will be estimated online together with a scaling factor which automatically calibrates the measurements of the pitot-static tube. Eventually the estimator will be tested using simulation results from a fixed wing UAV simulator.

II. Kinematics

The UAV's kinematics are given by (see Beard and McLain [2, p.36]):

$$\boldsymbol{a}^b = \dot{\boldsymbol{v}}^b + \boldsymbol{\omega}^b_{\boldsymbol{b/i}} \times \boldsymbol{v}^b \tag{1}$$

where $\boldsymbol{v}^b = (u, v, w)^T$ is the velocity vector of the aircraft relative to the earth decomposed in Body frame, $\boldsymbol{\omega}^b_{b/i}$ is the vector of the angular velocities between the inertial frame and the body frame decomposed in the body frame, and $\boldsymbol{a}^b$ is a vector with the UAV's accelerations measured in the Body frame by it's accelerometers. The so called "wind triangle" denotes the relationship between velocity over ground $\boldsymbol{v}^n$, relative velocity of the aircraft to the surrounding airmass $\boldsymbol{v}^n_r$ and wind velocity $\boldsymbol{v}^n_w$ relative to the earth in the inertial frame.

$$\boldsymbol{v}^n_r = \boldsymbol{v}^n - \boldsymbol{v}^n_w \tag{2}$$

To convert this to the Body frame, this equation is multiplied with the rotation matrix $\boldsymbol{R}^b_n$

$$\boldsymbol{v}^b_r = \boldsymbol{v}^b - \boldsymbol{R}^b_n v^n_w = (u_r, v_r, w_r)^T \tag{3}$$

Knowing $\boldsymbol{v}^b_r$ allows the calculation of the angle of attack (AoA) α, the sideslip angle (SSA) β and the airspeed V_a :

$$\alpha = \tan^{-1}\left(\frac{w_r}{u_r}\right) \tag{4}$$

$$\beta = \sin^{-1}\left(\frac{v_r}{V_a}\right) \tag{5}$$

$$V_a = \| \boldsymbol{v}^b_r \| \tag{6}$$

III. Aerodynamics

Following Beard and McLain [2, p.49] the total z-acceleration decomposed in the Body z- axis f_z of a fixed-wing UAV is given by

$$f_z = a_z - g\cos(\phi)\cos(\theta) \tag{7}$$

$$= \frac{\rho S}{2m} V_a^2 \left(-C_L(\alpha)\cos(\alpha) - C_D(\alpha)\sin(\alpha)\right) \tag{8}$$

where ρ is the density of the air, S is the surface area of the wing and m is the mass of the UAV. $C_L(\alpha)$ and $C_D(\alpha)$ are the lift and drag coefficients, which have a non-linear dependency on α. For small angles of attack this can be linearized as follows:

$$C_L(\alpha) = C_{L,0} + \alpha C_{L,\alpha} \tag{9}$$

$$C_D(\alpha) = C_{D,0} + \alpha C_{D,\alpha} \tag{10}$$

Inserting (9) and (9) into equation (8) and applying a second order approximation yields:

$$f_z = -KV_a^2 \left(C_{L,0} + \alpha\left(C_{L,\alpha} + C_{D,0}\right) + \alpha^2\left(C_{D,\alpha} - \frac{C_{L,0}}{2}\right)\right) \tag{11}$$

Fixed wing aircrafts are designed in a way that minimizes drag and maximizes lift forces. Therefore drag coefficients are significantly lower than lift coefficients (often one order of magnitude or more, see i.e. [2, pp.278]) and their influence is negligible here. Since we are considering normal flight with low angles of attack ($|\alpha| < 10°$) and $C_{L,0}$ is normally much smaller than $C_{L,\alpha}$, the quadratic term $-\frac{C_{L,0}}{2}\alpha^2$ can be omitted here as well. We then get the simpler approximate aerodynamic lift model:

$$f_z = -KV_a^2 \left(C_{L,0} + \alpha C_{L,\alpha}\right) \tag{12}$$

Solving this equation for α provides an alternative method to estimate the angle of attack compared to using (3) - (4), since f_z is measured by an accelerometer.

IV. Wind modeling

In the following we use a time-discrete model where k denotes the current time index and Δx_k the difference between x_k and x_{k-1}. The wind velocity $\boldsymbol{v}^n_w$ is assumed to be the sum of a low frequency part $\boldsymbol{v}^n_s$ and a high frequency turbulent part $\boldsymbol{v}^n_t$ [2, pp.55].

$$\boldsymbol{v}^n_{w,k} = \boldsymbol{v}^n_{s,k} + \boldsymbol{v}^n_{t,k} \tag{13}$$

$$\Delta \boldsymbol{v}^n_{s,k} \approx 0 \tag{14}$$

The turbulent wind velocity is modeled by the Dryden wind model [1]

$$\Delta \boldsymbol{v}^n_{t,k} = -\Delta T V_{a,k} \begin{pmatrix} \frac{u^n_t}{L_u} \\ \frac{v^n_t}{L_v} \\ \frac{w^n_t}{L_w} \end{pmatrix}\Bigg|_k + \begin{pmatrix} \sigma_u\sqrt{2\Delta T\frac{V_a}{L_u}}\eta_u \\ \sigma_v\sqrt{2\Delta T\frac{V_a}{L_v}}\eta_v \\ \sigma_w\sqrt{2\Delta T\frac{V_a}{L_w}}\eta_w \end{pmatrix}\Bigg|_k \tag{15}$$

where ΔT is the sampling period and the η_i are independent Gaussian white noise processes. The spectral wavelengths L_i are given by:

$$L_{u,k} = L_{v,k} = \frac{h_k}{(0.177 + 0.000823 * h_k)^{1.2}} \tag{16}$$

$$L_{w,k} = h_k \tag{17}$$

where h_k is the current altitude. The noise amplitudes σ_i are given by:

$$\sigma_{u,k} = \sigma_{v,k} = V_{w,G}\frac{0.1}{(0.177 + 0.000823 \cdot h_k)^{0.4}} \tag{18}$$

$$\sigma_w = 0.1 \cdot V_{w,G} \tag{19}$$

where $V_{w,G}$ is the wind speed measured 6 meters above ground.

V. Sensors and Estimation Structure

Assume the UAV is equipped with the following basic sensor suite:

- GNSS providing velocity over ground measurements
- IMU measuring total accelerations as well as angular rates to the attitude and heading reference system (AHRS) for attitude estimation.
- Pitot-static tube providing measurements of the relative airspeed in longitudinal direction u^m_r.

The cascaded estimator structure is similar to [6] and is depicted in Figure 1. As in [6] it's stability properties are inherited from the individual modules, which are:

- AHRS estimates the attitude (roll, pitch and yaw angles ϕ, θ, ψ) and also compensates for the gyroscope and accelerometers biases resulting in $\boldsymbol{\omega}$ and $\boldsymbol{a}$. A popular approach here is the EKF and non-linear observers [2], [8], [5].

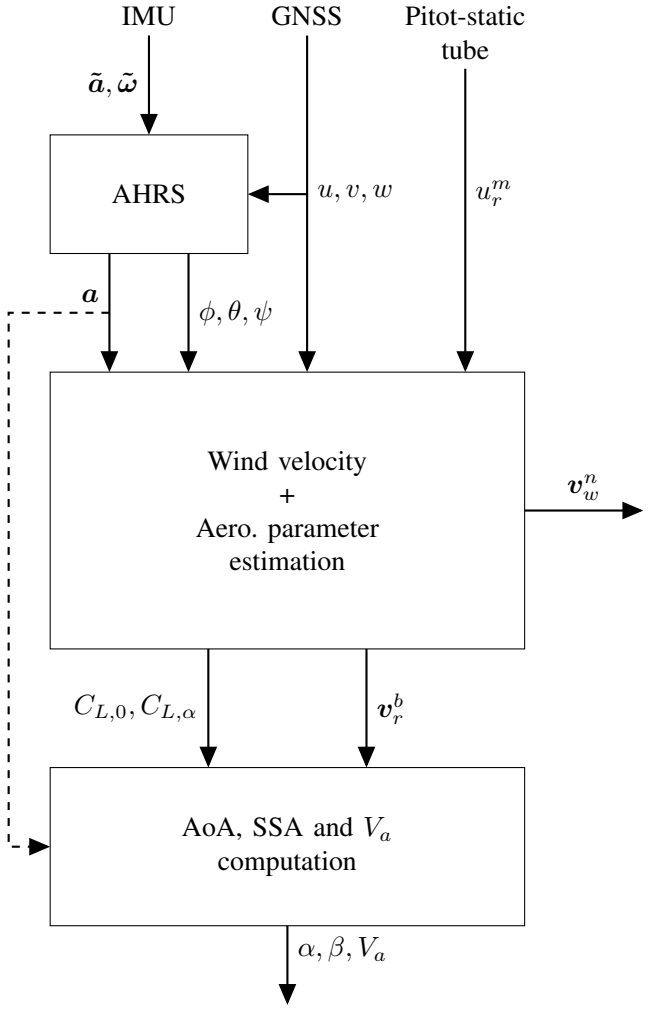

Fig. 1: System Layout

- The "wind velocity observer" estimates the steady wind velocity $\boldsymbol{v}_s^n$ and the turbulent wind velocity $\boldsymbol{v}_t^n$ as well as the lift coefficients $C_{L,0}.C_{L,\alpha}$ using the kinematic model in section II, the aerodynamic model in section III and the wind model described in section IV.
- In the "AoA, SSA and V_a computation" module the airflow variables are calculated using the estimated relative airspeed vector and (4) - (6). Note that the computation of α can also be done using the estimated lift coefficients and the z-acceleration and (12).

VI. Wind Velocity and Lift coefficient estimator

In section IV the wind velocity was modeled as the sum of a low frequency part and a high frequency part. To estimate the steady wind velocity we will use a similar idea as in [6] and combine the kinematic model derived in section II with the measurements from the pitot-static tube u_r^m and the x-component of the GNSS velocity rotated to the body frame u^b.

For the turbulent wind velocity we will combine the Dryden model with the aerodynamic model which will allow us to estimate the lift coefficients $C_{L,0}$ and $C_{L,\alpha}$. These couple the vertical acceleration to the angle of attack α via (12) and the airspeed V_a. Unfortunately in both α and V_a the sum of the turbulent and the steady wind velocity appears and makes it challenging to observe them separately. However in practice a fast change in acceleration can be interpreted in (12) to be due to a change in angle of attack, which has higher frequency components, than the steadier airspeed. Therefore we can introduce a frequency separation, by defining $\bar{\boldsymbol{v}}_{\boldsymbol{r}}^{\boldsymbol{b}}$ and $\bar{V}_a$ as low frequency versions of $\boldsymbol{v}_r^b$ and V_a which are independent of $\boldsymbol{v}_t^n$.

$$\bar{\boldsymbol{v}}_{\boldsymbol{r}}^{\boldsymbol{b}} = \boldsymbol{v}^b - \boldsymbol{R}_n^b \boldsymbol{v}_s^n \tag{20}$$

$$\bar{V}_a = \left\| \bar{\boldsymbol{v}}_{\boldsymbol{r}}^{\boldsymbol{b}} \right\| \tag{21}$$

Replacing V_a by $\bar{V}_a$ in (12) results in the approximation

$$f_z = -K\bar{V}_a^2(\boldsymbol{v}_s^n)\left(C_{L,0} + \alpha(\boldsymbol{v}_s^n, \boldsymbol{v}_t^n)C_{L,\alpha}\right) \tag{22}$$

This simplifies the aerodynamic model (12) with respect to $\boldsymbol{v}_t^n$ and also, as we will show later, provides different gradients when differentiating (22) with respect to $\boldsymbol{v}_s^n$ and $\boldsymbol{v}_t^n$. This allows the distinction between the two wind velocities within the estimator. Because of the non-linear nature of the used models, an Extended Kalman Filter (EKF) [7] is applied here . The EKF has a predictor - corrector structure, where the state equation is used for predicting the state $\boldsymbol{x}_{k|k-1}$ at the time step k based on the previous state $\boldsymbol{x}_{k-1|k-1}$ and the input u_k. The estimated state $\boldsymbol{x}_{k|k}$ is then obtained by correcting predicted state with the measurement $\boldsymbol{z}_k$.

A. State equations

The states to be estimated are the steady and the turbulent wind velocities in the inertial frame, the two lift coefficients and a scaling factor governing pitot-static tube calibration.

$$\boldsymbol{x} = \begin{bmatrix} u_s^n & v_s^n & w_s^n & u_t^n & v_t^n & w_t^n & C_{L_0} & C_{L_\alpha} & \gamma \end{bmatrix}^T$$

All wind velocities are decomposed in inertial frame and all relative and ground velocities are decomposed in body frame, in order to simplify the notation the identifier of the frame will be omitted from now on (e.g. $\boldsymbol{v}_s = \boldsymbol{v}_s^n, v_r = v_r^b$). Inputs to the observer are the velocity over ground in the body frame, the Euler angles, the measurement of the pitot tube and the altitude.

$$\boldsymbol{u} = \begin{bmatrix} u^b & v^b & w^b & \phi & \theta & \psi & u_r^m & h \end{bmatrix}^T$$

The steady wind velocities, the lift coefficients and the scaling factor are assumed to be slowly time varying ($\Delta x_i \approx 0$). According to equation (15) the turbulent wind $\boldsymbol{v}_{t,k}$ is dependent on the previous state as follows:

$$\Delta \boldsymbol{v}_{t,k-1} = -\boldsymbol{v}_{t,k-1}\Delta T \left(\begin{matrix} \frac{\bar{V}_a}{L_u} \\ \frac{\bar{V}_a}{L_v} \\ \frac{\bar{V}_a}{L_w} \end{matrix} \right) \Bigg|_{\substack{\boldsymbol{u}_{k-1} \\ \boldsymbol{x}_{k-1|k-1}}} \tag{23}$$

Which results in the following state transition function:

$$\begin{aligned}\boldsymbol{x}_{k|k-1} =& \boldsymbol{f}(\boldsymbol{x}_{k-1|k-1}) \\ =& \boldsymbol{x}_{k-1|k-1} + \\ & \begin{bmatrix}0 & 0 & 0 & \Delta v_{t,k-1} & 0 & 0 & 0\end{bmatrix}^T \end{aligned} \tag{24}$$

For the EKF the Jacobian of the state transition function is needed, which is given by:

$$\boldsymbol{F}_{k-1} = \left.\frac{\delta \boldsymbol{f}(\boldsymbol{x},\boldsymbol{u})}{\delta \boldsymbol{x}}\right|_{\substack{\boldsymbol{u}_{k-1} \\ \boldsymbol{x}_{k-1|k-1}}} = \begin{bmatrix} \boldsymbol{I}_{[3]} & \boldsymbol{0}_{[3,3]} & \boldsymbol{0}_{[3,3]} \\ \frac{\delta \boldsymbol{f}}{\delta \boldsymbol{v}_s} & \frac{\delta \boldsymbol{f}}{\delta \boldsymbol{v}_t} & \boldsymbol{0}_{3,3} \\ \boldsymbol{0}_{[3,3]} & \boldsymbol{0}_{[3,3]} & \boldsymbol{I}_{[3]} \end{bmatrix} \tag{25}$$

where $\boldsymbol{I}_{[m]}$is an identity matrix with dimension m and $\boldsymbol{0}_{[n,m]}$ is a matrix filled with zeros of dimensions (n, m). During one prediction step of the Dryden model, the airspeed is assumed to be slowly changing compared to the turbulent wind velocity. Therefore the definition of the slowly time varying airspeed (21) is used.

$$\frac{\delta \bar{V}_a}{\delta \boldsymbol{v}_t} = \boldsymbol{0} \tag{26}$$

Hence the sub-Jacobians are calculated from (23) as follows:

$$\frac{\delta \boldsymbol{f}}{\delta \boldsymbol{v}_t} = diag\left[1 - \Delta T \frac{\bar{V}_a}{L_u}, \quad 1 - \Delta T \frac{\bar{V}_a}{L_v}, \quad 1 - \Delta T \frac{\bar{V}_a}{L_w}\right] \tag{27}$$

$$\frac{\delta \boldsymbol{f}}{\delta \boldsymbol{v}_s} = \begin{bmatrix} \frac{\Delta T u_t}{L_u}\frac{\delta \bar{V}_a}{\delta u_s} & \frac{\Delta T u_t}{L_u}\frac{\delta \bar{V}_a}{\delta v_s} & \frac{\Delta T u_t}{L_u}\frac{\delta \bar{V}_a}{\delta w_s} \\ \frac{\Delta T v_t}{L_v}\frac{\delta \bar{V}_a}{\delta u_s} & \frac{\Delta T}{L_v}\frac{\delta \bar{V}_a}{\delta v_s} & \frac{\Delta T v_t}{L_v}\frac{\delta \bar{V}_a}{\delta w_s} \\ \frac{\Delta T w_t}{L_w}\frac{\delta \bar{V}_a}{\delta u_s} & \frac{\Delta T w_t}{L_w}\frac{\delta \bar{V}_a}{\delta v_s} & \frac{\Delta T w_t}{L_w}\frac{\delta \bar{V}_a}{\delta w_s} \end{bmatrix} \tag{28}$$

where:

$$\frac{\delta \bar{V}_a}{\delta u_s} = \frac{\delta}{\delta u_s} \parallel \bar{\boldsymbol{v}}_{\boldsymbol{r}} \parallel \tag{29}$$

$$= \frac{1}{\parallel \bar{\boldsymbol{v}}_{\boldsymbol{r}} \parallel}\left(u_r \frac{\delta u_r}{\delta u_s} + v_r \frac{\delta v_r}{\delta u_s} + w_r \frac{\delta w_r}{\delta u_s}\right) \tag{30}$$

$$= -\bar{V}_a^{-1}(\boldsymbol{R}_{\boldsymbol{n}}^{\boldsymbol{b}} \boldsymbol{d_1})^T \bar{\boldsymbol{v}}_{\boldsymbol{r}} \tag{31}$$

$$\boldsymbol{d}_1^T = \begin{bmatrix}1 & 0 & 0\end{bmatrix} \tag{32}$$

The derivatives with respect to v_s and w_s are calculated similarly.

As can be seen in equation (15) the turbulence is modeled by colored noise, whose amplitude is changing with the altitude and the ground wind speed. This leads to a time varying covariance matrix:

$$\boldsymbol{Q}_k = diag\begin{pmatrix} a_{u_s} \\ a_{v_s} \\ a_{w_s} \\ a_{u_t}\sigma_{u,k}\sqrt{2\Delta T \frac{V_{a,k}}{L_{u,k}}} \\ a_{v_t}\sigma_{v,k}\sqrt{2\Delta T \frac{V_{a,k}}{L_{v,k}}} \\ a_{w_t}\sigma_{v,k}\sqrt{2\Delta T \frac{V_{a,k}}{L_{w,k}}} \\ a_{C_{L,0}} \\ a_{C_{L,\alpha}} \\ a_{\gamma} \end{pmatrix} \Delta T^2 \tag{33}$$

where the a_i are tuning factors.

B. Measurement Equations

The measurement vector is given by the total body z-acceleration and the body velocity in x-direction, which are affected by some measurement noise ν. The measurement noise is modeled as zero-mean Gaussian white noise:

$$\boldsymbol{z}_k = \begin{bmatrix} f_z \\ u^b \end{bmatrix} = \begin{bmatrix} a_z - g\cos(\theta)\cos(\phi) \\ u^b \end{bmatrix} + \boldsymbol{\nu}_k \tag{34}$$

The output function is obtained by using the wind triangle (3), the linearized aerodynamics (22) and (21).

$$\boldsymbol{h}(\boldsymbol{x},\boldsymbol{u}) = \begin{bmatrix} -K\bar{V}_a^2(C_{L_0} + C_{L_\alpha}\alpha) \\ \boldsymbol{d}_1 \boldsymbol{R}_n^b(\boldsymbol{v}_s + \boldsymbol{v}_t) + \gamma u_r^m \end{bmatrix} \tag{35}$$

where $K = \frac{\rho S}{2m}$.

The observation matrix is given by the Jacobian of the output function:

$$\boldsymbol{H}_k = \frac{\delta}{\delta \boldsymbol{x}}\left.\begin{bmatrix} -K\bar{V}_a^2(C_{L_0} + C_{L_\alpha}\alpha) \\ \boldsymbol{d}_1 \boldsymbol{R}_n^b(\boldsymbol{v}_s + \boldsymbol{v}_t) + \gamma u_r^m \end{bmatrix}\right|_{\substack{\boldsymbol{u}_{k-1} \\ \boldsymbol{x}_{k|k-1}}} = \frac{\delta}{\delta \boldsymbol{x}}\begin{bmatrix} h_1 \\ h_2 \end{bmatrix}$$

Since h_2 is linear the calculation of the Jacobian is straightforward. For h_1 some additional steps are necessary:

$$\begin{aligned}\frac{\delta}{\delta u_s}h_1 =& -K\frac{\delta \bar{V}_a^2}{\delta u_s}(C_{L_0} + C_{L_\alpha}\alpha) \\ & - K\bar{V}_a^2\left(C_{L_\alpha}\frac{\delta}{\delta u_s}\tan^{-1}\left(\frac{w_r}{u_r}\right)\right) \end{aligned} \tag{36}$$

$$\frac{\delta}{\delta u_s}\alpha = \frac{-R^b_{n_{(3,1)}}u_r + R^b_{n_{(1,1)}}w_r}{u_r^2 + w_r^2} \tag{37}$$

$$\begin{aligned}\frac{\delta}{\delta u_s}h_1 =& 2K(\boldsymbol{R}_{\boldsymbol{n}}^{\boldsymbol{b}}\boldsymbol{d_1})^T\bar{\boldsymbol{v}}_{\boldsymbol{r}}(C_{L_0} + C_{L_\alpha}\alpha) \\ & + \frac{-R^b_{n_{(3,1)}}u_r + R^b_{n_{(1,1)}}w_r}{u_r^2 + w_r^2} \end{aligned} \tag{38}$$

where $R^b_{n_{(i,j)}}$ denotes the element (i, j) of the rotation matrix. The other derivitatives are calculated in the same manner:

$$\begin{aligned}\frac{\delta}{\delta v_s}h_1 =& 2K(\boldsymbol{R}_{\boldsymbol{n}}^{\boldsymbol{b}}\boldsymbol{d_2})^T\bar{\boldsymbol{v}}_{\boldsymbol{r}}(C_{L_0} + C_{L_\alpha}\alpha) \\ & + \frac{-R^b_{n_{(3,2)}}u_r + R^b_{n_{(1,2)}}w_r}{u_r^2 + w_r^2} \end{aligned} \tag{39}$$

$$\begin{aligned}\frac{\delta}{\delta w_s}h_1 =& 2K(\boldsymbol{R}_{\boldsymbol{n}}^{\boldsymbol{b}}\boldsymbol{d_3})^T\bar{\boldsymbol{v}}_{\boldsymbol{r}}(C_{L_0} + C_{L_\alpha}\alpha) \\ & + \frac{-R^b_{n_{(3,3)}}u_r + R^b_{n_{(1,3)}}w_r}{u_r^2 + w_r^2} \end{aligned} \tag{40}$$

where $\boldsymbol{d}_2^T = [0, 1, 0]$ and $\boldsymbol{d}_3^T = [0, 0, 1]$.

For the deriviatives with respect to $\boldsymbol{v}_t$, (26) is used again, and therefore

$$\frac{\delta}{\delta u_t}h_1 = -K\bar{V}_a^2\left(C_{L_\alpha}\frac{\delta}{\delta u_t}\tan^{-1}\left(\frac{w_r}{u_r}\right)\right) \tag{41}$$

$$= K\bar{V}_a^2 C_{L_\alpha}\frac{R^b_{n_{(3,1)}}u_r - R^b_{n_{(1,1)}}w_r}{w_r^2 + u_r^2} \tag{42}$$

and in the same manner:

$$\frac{\delta}{\delta v_t} h_1 = K\bar{V}_a^2 C_{L_\alpha} \frac{R^b_{n_{(3,2)}} u_r - R^b_{n_{(1,2)}} w_r}{w_r^2 + u_r^2} \tag{43}$$

$$\frac{\delta}{\delta w_t} h_1 = K\bar{V}_a^2 C_{L_\alpha} \frac{R^b_{n_{(3,3)}} u_r - R^b_{n_{(1,3)}} w_r}{w_r^2 + u_r^2} \tag{44}$$

This results in the following observation matrix:

$$\boldsymbol{H}_k = \begin{bmatrix} \frac{\delta h_1}{\delta \boldsymbol{v}_s}^T & \frac{\delta h_1}{\delta \boldsymbol{v}_t}^T & -K\bar{V}_a^2 & -K\bar{V}_a^2\alpha & 0 \\ \boldsymbol{d}_1^T \boldsymbol{R}_n^b & \boldsymbol{d}_1^T \boldsymbol{R}_n^b & 0 & 0 & u_r^m \end{bmatrix} \tag{45}$$

$$\frac{\delta h_1}{\delta \boldsymbol{v}_\tau}^T = \begin{bmatrix} \frac{\delta h_1}{\delta u_\tau} & \frac{\delta h_1}{\delta v_\tau} & \frac{\delta h_1}{\delta w_\tau} \end{bmatrix} \qquad \tau \in \{s, t\} \tag{46}$$

The second row of the observation matrix corresponds to the measurement equation in [6]. In that paper it was shown analytically that the wind velocity is observable when sufficient changes in the pitch and yaw angles of the UAV occur. Simulations will show that in this approach attitude changes are also necessary during the initialization phase of the EKF. When accurate estimates of the lift coefficients are obtained periodical attitude changes are only needed to avoid drift in these coefficients or to detect changes in them.

VII. Simulation Setup

A. UAV Simulation

All simulations were performed using a simulation of the X8 flying wing and a simulated autopilot. The simulator and the autopilot are based on Beard and McLain [2, Chap. 4 and 6] and implemented in Matlab / Simulink. In the aircraft simulation a more complex non-linear model of the aerodynamics is used (for details see [2, pp.44]). The aerodynamic forces are thus given by:

$$\zeta = \frac{1 + e^{-M(\alpha-\alpha_0)} + e^{M(\alpha+\alpha_0)}}{\left(1 + e^{-M(\alpha-\alpha_0)}\right)\left(1 + e^{M(\alpha+\alpha_0)}\right)} \tag{47}$$

$$C_L(\alpha) = (1-\zeta)(C_{L,0} + C_{L,\alpha}\alpha) + \zeta(2\,\mathrm{sign}(\alpha)\sin(\alpha)^2\cos(\alpha)) \tag{48}$$

$$F_L = \frac{1}{2}\rho V_a^2 S(C_L(\alpha) + C_{L,q}c/(2V_a)q + C_{L,\delta_e}\delta_e) \tag{49}$$

$$C_{D,\alpha} = C_{D,p} + (1-\zeta)\frac{(C_{L,0} + C_{L,\alpha}\alpha)^2}{\pi e(b^2/S)} + \zeta 2\,\mathrm{sign}(\alpha)\sin(\alpha)^3 \tag{50}$$

$$F_D = \frac{1}{2}\rho V_a^2 S \left(C_{D,\alpha} + C_{D,q}\frac{c}{2V_a}q + C_{D,\delta_e}|\delta_e|\right) \tag{51}$$

$$\begin{pmatrix} f_x \\ f_z \end{pmatrix} = \begin{pmatrix} \cos\alpha & -\sin\alpha \\ \sin\alpha & \cos\alpha \end{pmatrix} \begin{pmatrix} -F_D/m \\ -F_L/m \end{pmatrix} \tag{52}$$

where M and α_0 are positive constants, c is the mean aerodynamic chord of the wing, q is the pitch-rate and δ_e is the elevator deflection and $C_{L,q}, C_{L,\delta_e}, C_{D,q}, C_{D,\delta_e}$ are their respective lift and drag coefficients.

Wind velocity is simulated following Beard and McLain [2, pp.55] as the sum of a steady and a turbulent wind velocity component, where the turbulence is generated by passing white noise through a low pass filter. The filter is designed in the way described in section IV according to the Dryden model. The steady wind velocity and the wind velocity at 6m above ground, needed for the turbulence generation, were set to $6m/s$, the wind direction was set to $90°$.

B. Initial Conditions and Tuning

The initial condition for the state vector was set to:

$$\boldsymbol{x}_0 = \begin{bmatrix} 0 & 0 & 0 & 0 & 0 & 0 & 0 & 1 & 1 \end{bmatrix}^T \tag{53}$$

The inital condition for the state covariance matrix was set to:

$$\boldsymbol{P}_0 = diag\begin{bmatrix} 10^{-2} & 10^{-2} & 10^{-4} & 10^{-5} & 10^{-5} \\ 10^{-5} & 10^{-5} & 10^{-1} & 10^{-8} & \end{bmatrix} \tag{54}$$

The tuning factors of the process noise covariance matrix $\boldsymbol{Q}$ were set to:

$$a = \begin{bmatrix} 10^{-7} & 10^{-7} & 10^{-10} & 5\cdot 10^2 & 5\cdot 10^2 \\ 2\cdot 10^2 & 10^{-6} & 10^{-10} & 10^{-15} & \end{bmatrix} \tag{55}$$

The covariance matrix of the measurement noise was chosen to:

$$\boldsymbol{R} = diag(1, 0.6) \tag{56}$$

This covariance matrix is important in tuning the EKF. It quantifies the expected uncertainties in the measurement equation induced by noise in the sensors and errors within the attitude estimation. The measurement noise ν is modeled as band limited white noise with the following variances:

$$\sigma_\nu = \begin{bmatrix} 0.1 \\ 0.1 \end{bmatrix} \tag{57}$$

For the measurement of the pitot-static tube the measurement noise was model as Gaussian white noise with a variance of 0.1. It was assumed in the simulation that the AHRS system supplies the estimator with accurate attitude angles with negligible noise levels.

C. Inputs

Here we simulate a normal take off and some circles, which are often performed by UAV pilots before handing control over to an autopilot. The UAV performs one circle per minute. The UAV is commanded to fly at an altitude of $150m$, with a course angle of $60°$. Later the UAV changes altitude to $250m$ and course $90°$ at two different time instants. The input signals can be seen in Figure 2 and Figure 3.

VIII. Simulation Results

A. Wind Velocities and Airspeed

Figure 4 show the wind velocity estimates in x, y and z direction in NED frame and their respective references. As can be seen, the wind velocity estimation is very accurate for the z-velocity. This results from the very tight coupling to the z-acceleration through α. The velocities in x and y direction

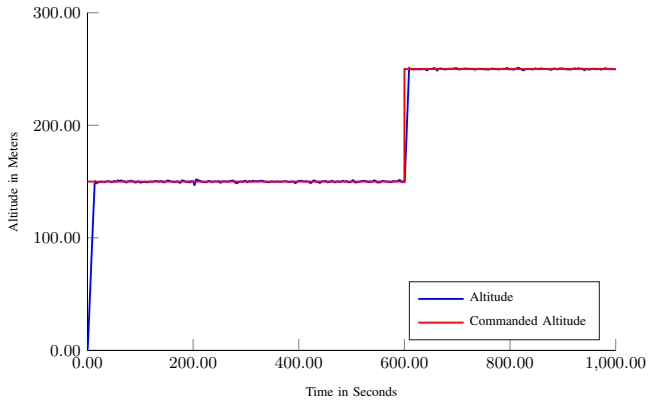

Fig. 2: Commanded and resulting altitude of the UAV

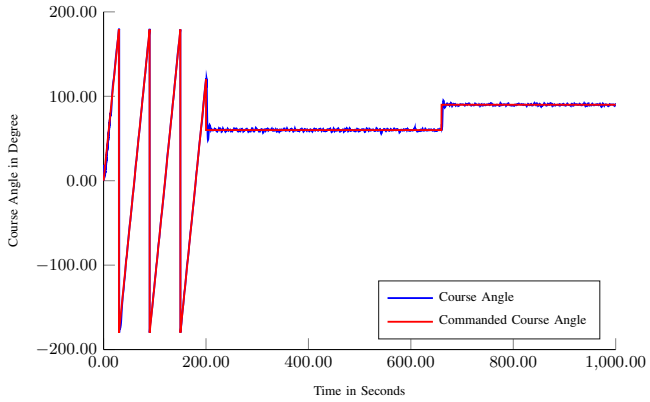

Fig. 3: Commanded and resulting course angle of the UAV

rely more on the measurement of the pitot-static tube, since the coupling to the z-acceleration is fairly weak through the denominator in (4). Therefore change in yaw angle is needed to provide measurement updates in both directions. This can be seen in Figure 4: In the intermediate part of the flight the UAV is moving in north east direction (course $60°$) during this part the estimates for wind in east direction are fairly good where as in north direction have a larger error. This error increased even more when the aircraft is moving in east direction during the second part (time $\leq 660s$) of the flight. Notable is that the steady wind velocity estimate in north direction is still reasonably accurate.

Using the wind velocity estimates and the GNSS velocity, the airspeed V_a can be calculated using equation (6). The result is shown in Figure 5. The estimated airspeed is also compared to an estimate from previous work [6], which only uses pitot tube and GNSS measurements and not the accelerometers. The root mean square error (RMSE) for the wind estimator proposed here is $0.23m/s$, which is an improvement compared to the pitot - tube only estimator which has a RMSE of $0.72m/s$.

B. Lift coefficients and Angle of Attack

Figure 6 shows the estimates of the lift coefficients. The dynamic lift coefficient estimate $C_{L,\alpha}$ remains at a small offset from its true value, but this is reasonably small. The

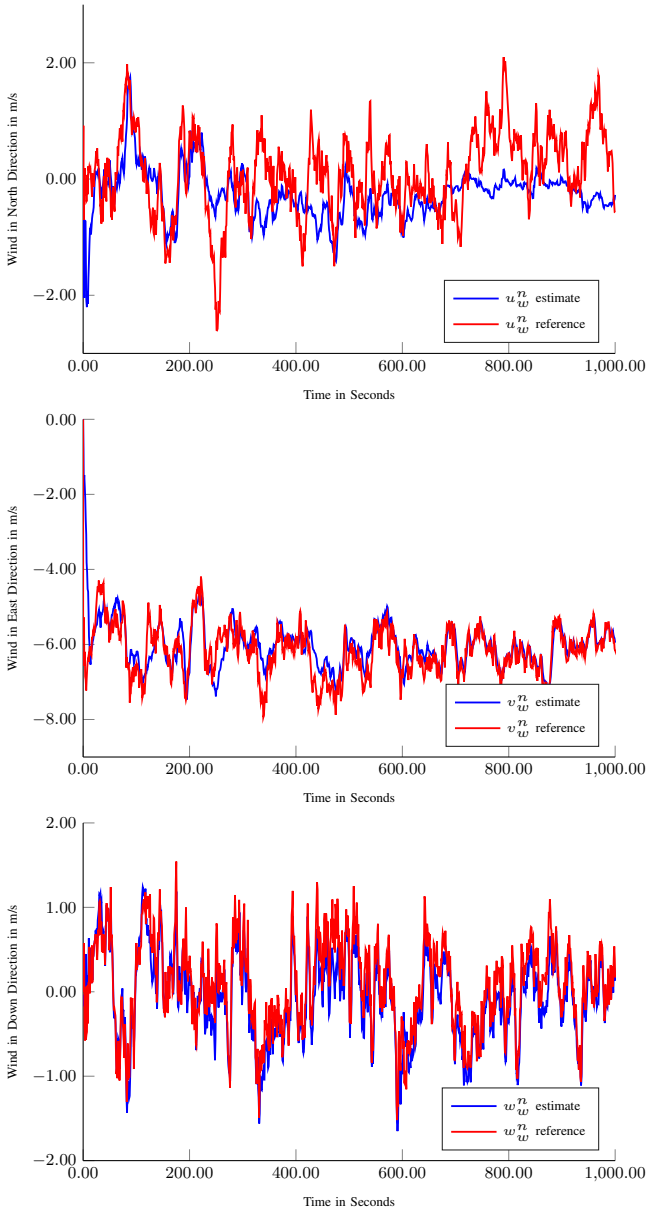

Fig. 4: Wind velocity estimates (blue) in NED frame and true values (red)

static lift coefficient estimate $C_{L,0}$ shows some larger relative errors. This could be due to modeling errors induced by the linearization done in section III. However, as will be shown later, the influence of these errors on the angle of attack estimate is minor. The black dashed lines show the confidence intervals of the estimate (3σ). For both coefficients these intervals are quite narrow and indicates a high confidence in the estimates of the EKF. Notice that $C_{L,\alpha}$ and $C_{L,0}$ are drifting slowly over time. This occurs because due to the constant pitch angle no information from the pitot tube over the wind velocity in down direction is available. This increases the uncertainty in the lift coefficients and the wind velocity in z-direction over time. To resolve this one could either perform periodic changes in altitude, choose lower

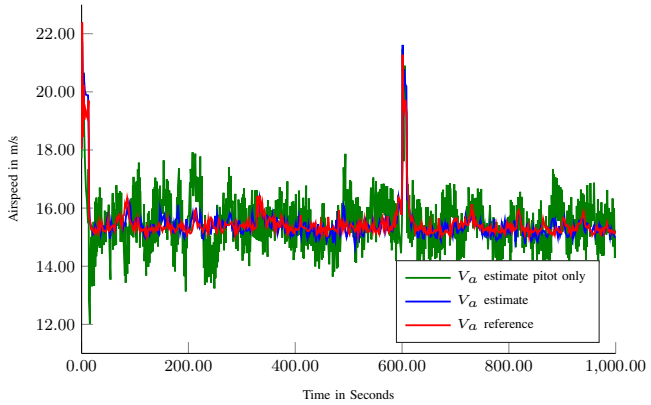

Fig. 5: Total Airspeed estimate (blue), reference (red) and estimate of pitot-static tube only estimator of [6] (green), $RMSE = 0.23m/s, RMSE_{pitot} = 0.72m/s$

process noise covariance values or freeze the lift coefficients. This also depends whether the coefficient is likely to change or not.

As mentioned in section V the angle of attack can be calculated in two ways either by using the lift coefficients, the z- acceleration and V_a solving equation (12) or by using the airspeed vector $\boldsymbol{v}_r^b$ using (4). Figure 7 shows a comparison of these two methods. The calculation via the first method yields better results compared to the second method, which might be due to the fact that the tuning was aiming on slowly drifting lift coefficients, which leads to higher drift on the steady wind velocities when no attitude changes occur. Note that although the are some errors in the lift coefficient estimates, these only induce small errors in the angle of attack estimate.

Figure 8 shows the estimated angle of attack, calculated by solving equation (12) for α, the estimate obtained by only using pitot-tube data and GNSS data as well as the true value from the simulation. The root mean square error (RMSE) for the wind estimator proposed here is $0.33°$, which is an significant improvement compared to the pitot - tube only estimator which has a RMSE of $2.04°$.

C. Scaling Factor

Figure 9 shows the estimate of the pitot tube scaling factor γ. The scaling factor rises quickly to a region around to its reference value and remains there for the whole simulation run. Some small changes occur, which are due to measurement noise and uncertainty in the other state estimates.

D. Sideslip Angle

For completeness also the estimated Sideslip Angle is shown in Figure 10. It is calculated from equation (5). Compared to [6] there are only slight improvements in the estimation performance. This was expected since the lateral acceleration is not included in the estimation, and additional information within the estimator can only be obtained from the wind model regarding the lateral wind velocity in body

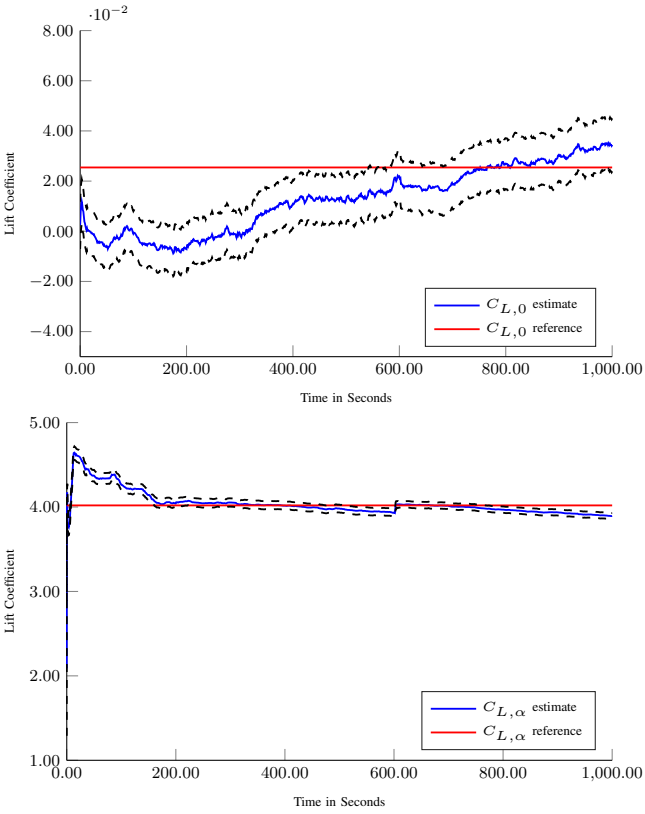

Fig. 6: Estimates of static and dynamic lift coefficient, dashed black lines indicate 3 σ intervall

frame. This could be improved by including a model of the lateral aerodynamics and using f_y accelerometer measurements.

IX. Conclusion

This paper studies the estimation of wind velocity, in order to compute angle of attack, sideslip angle and wind velocity, using kinematic and aerodynamic relationships as well as a model of turbulent winds. The wind is modeled as a sum of steady, slowly changing wind and turbulent wind, for which the Dryden model was applied. As sensors only standard sensors typical of a UAV, consisting of GNSS, IMU and a pitot-static tube, are used. The models and measurement data were combined in an Extended Kalman Filter.

The estimator was tested using a fixed wing UAV simulator and an autopilot model. Simulation results showed generally good performance in estimation of the wind velocities and the lift coefficients. This leads to significant improvements of the angle of attack and airspeed estimates compared to [6]. The estimate of the sideslip angle shows also improvements, but these are limited since no information about the lateral aerodynamics and lateral accelerometer measurements were used within the estimator.

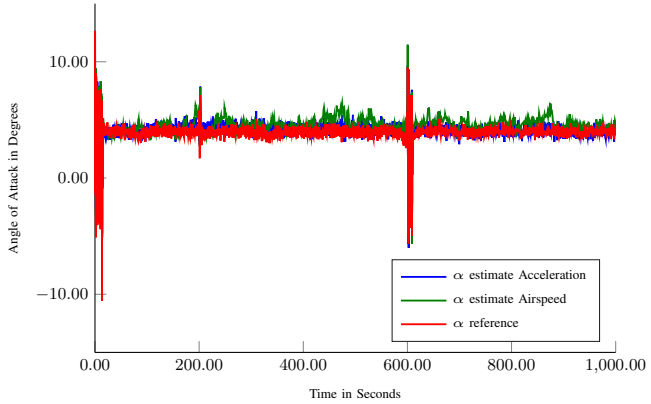

Fig. 7: Comparison of Angle of Attack calculation methods, $RMSE_{Acc} = 0.33°, RMSE_{Air} = 0.85°$

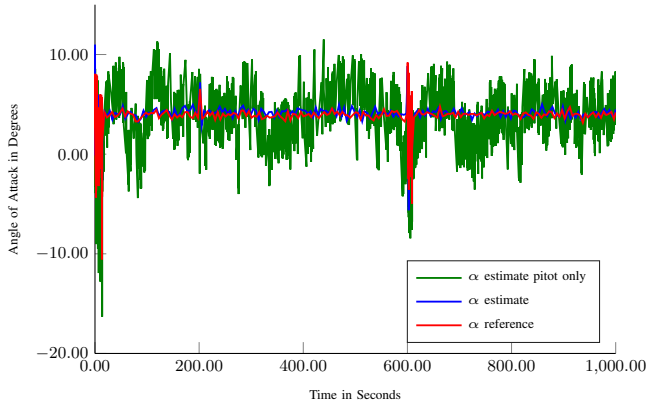

Fig. 8: Angle of Attack estimation(blue), reference (red) and estimate of pitot-static tube only estimator of [6] (green) $RMSE = 0.33°, RMSE_{pitot} = 2.04°$

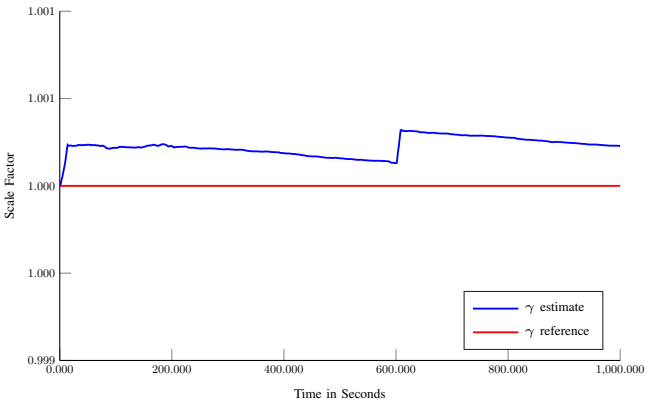

Fig. 9: Estimate of the pitot tube scaling factor γ

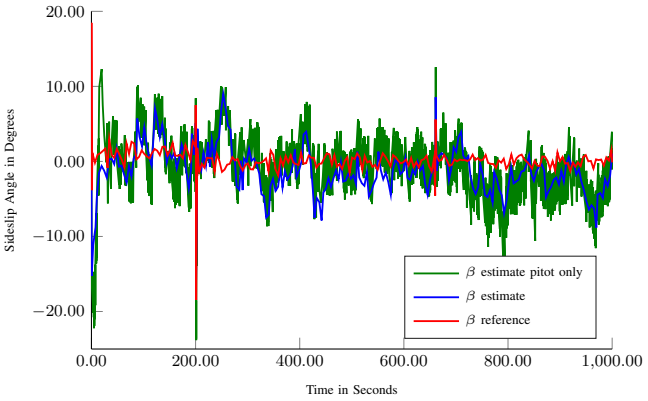

Fig. 10: Sideslip angle estimation (blue), reference (red) and estimate of pitot-static tube only estimator of [6] (green), $RMSE = 3.21°, RMSE_{pitot} = 3.50°$

X. Acknowledgments

This project has received funding from the European Unions Horizon 2020 research and innovation programme under the Marie Sklodowska-Curie grant agreement No 642153. The research was also funded by the Research Council of Norway through the Centres of Excellence funding scheme, grant number 223254 NTNU AMOS.
We would like to thank Kristoffer Gryte for the development of the UAV simulator.

References

[1] MIL-STD-1797A: Flying Qualities of Piloted Aircraft. Technical report, 2004.

[2] Randal W. Beard and Timothy W. McLain. *Small Unmanned Aircraft: Theory and Practice*. Princeton University Press, 2012.

[3] Am Cho, Jihoon Kim, Sanghyo Lee, and Changdon Kee. Wind estimation and airspeed calibration using a UAV with a single-antenna GPS receiver and pitot tube. *IEEE Trans. Aerosp. Electron. Syst.*, 47(1):109–117, 2011.

[4] Jean-philippe Condomines, Murat Bronz, and Gautier Hattenberger. Experimental Wind Field Estimation and Aircraft Identification Experimental Wind Field Estimation and Aircraft Identification. In *IMAV 2015 Int. Micro Air Veh. Conf. Flight Compet.*, 2015.

[5] Havard Fjær Grip, Thor I. Fossen, Tor A. Johansen, and Ali Saberi. Nonlinear observer for GNSS-aided inertial navigation with quaternion-based attitude estimation. In *Am. Control Conf.*, pages 272–279, jun 2013.

[6] Tor A Johansen, Andrea Cristofaro, Kim Sørensen, Jakob M Hansen, and Thor I Fossen. On estimation of wind velocity , angle-of-attack and sideslip angle of small UAVs using standard sensors. In *Int. Conf. Unmanned Aircr. Syst.*, Denver, 2015.

[7] R. E. Kalman and R. S. Bucy. New results in linear filtering and prediction theory. *J. Basic Eng.*, 83(1):95–108, 1961.

[8] Derek B Kingston and Randal W. Beard. Real-time Attitude and Position Estimation for Small UAVs using Low-cost Sensors. *Proc. AIAA Unmanned Unltd. Tech. Conf. Work. Exhib.*, pages 2004–6488, 2004.

[9] Makoto Kumon, Ikuro Mizumoto, Zenta Iwai, and Masanobu Nagata. Wind estimation by unmanned air vehicle with delta wing. In *Proc. - IEEE Int. Conf. Robot. Autom.*, volume 2005, pages 1896–1901. IEEE, 2005.

[10] Jack W Langelaan, Nicholas Alley, and James Neidhoefer. Wind Field Estimation for Small Unmanned Aerial Vehicles. *J. Guid. Control Dyn.*, 34:1016–1030, 2011.

[11] Hao Long and Shujie Song. Method of Estimating Angle-of-Attack and Sideslip Angel Based on Data Fusion. In *2009 Second Int. Conf. Intell. Comput. Technol. Autom.*, volume 1, pages 641–644. IEEE, 2009.

[12] Matthew B. Rhudy, Trenton Larrabee, Haiyang Chao, Yu Gu, and Marcello Napolitano. UAV Attitude, Heading, and Wind Estimation Using GPS/INS and an Air Data System. In *AIAA Guid. Navig. Control Conf.*, number 5201, pages 1–11, 2013.

[13] Andres Rodriguez, Evan Andersen, Justin Bradley, and Clark Taylor. Wind Estimation Using an Optical Flow Sensor on a Miniature Air Vehicle. In *AIAA Guid. Navig. Control Conf. Exhib.*, volume 6614, pages 1–8, Reston, Virigina, aug 2007. American Institute of Aeronautics and Astronautics.

[14] Mohammad Shaqura and Christian Claudel. A hybrid system approach

to airspeed, angle of attack and sideslip estimation in Unmanned Aerial Vehicles. In *Int. Conf. Unmanned Aircr. Syst. ICUAS 2015*, pages 723–732, 2015.

[15] Pengzhi Tian and Haiyang Chao. UAV Flight Test Evaluation of Fusion Algorithms for Angle of Attack and Sideslip Angle. In *AIAA Guid. Navig. Control Conf.*, number 0645, 2016.